The effects of platinum dispersion and Pt state on catalytic properties of Pt/Al₂O₃ in NH₃ oxidation

Elena M. Slavinskaya,[a] Lidiya S. Kibis,[a] Olga A. Stonkus,[a] Dmitry A. Svintsitskiy,[a] Andrei I. Stadnichenko,[a] Elizaveta A. Fedorova,[a] Anatolii V. Romanenko,[a] Vasyl Marchuk,[b] Dmitry E. Doronkin,[b,c] Andrei I. Boronin*[a]

[a]   Dr. E.M. Slavinskaya, Dr. L.S. Kibis, Dr. O.A. Stonkus, Dr. D.A. Svintsitskiy, Dr. A.I. Stadnichenko, Dr. A.V. Romanenko, E.A. Fedorova, Prof. Dr. A.I.
        Boronin
        Boreskov Institute of Catalysis SB RAS
        Pr. Lavrentieva 5, 630090 Novosibirsk, Russia
        E-mail: boronin@catalysis.ru
[b]   V. Marchuk, Dr. D.E. Doronkin,
        Institute for Chemical Technology and Polymer Chemistry
        Karlsruhe Institute of Technology (KIT),
        Engesserstr. 20, 76131 Karlsruhe, Germany
        E-Mail: dmitry.doronkin@kit.edu
[c]   Dr. D.E. Doronkin
        Institute of Catalysis Research and Technology
        Karlsruhe Institute of Technology (KIT)
        Hermann-von-Helmholtz-Platz 1, 76344 Eggenstein-Leopoldshafen, Germany

        Supporting information for this article is given via a link at the end of the document.

Abstract: Dependence of NH_3 oxidation on the state and dispersion of Pt species in Pt/γ-Al_2O_3 catalysts was investigated. Prereduced Pt/γ-Al_2O_3 catalysts containing Pt^0 nanoparticles exhibited significantly higher activity than preoxidized ones with the same Pt dispersion. The most significant improvement of the catalytic activity (TOF increased by 30 times) was observed when the size of Pt^0 particles increased from ~1 to ~8 nm. N_2 selectivity was found to be mainly determined by the reaction temperature, with a minor influence of Pt particle size. Preoxidized catalysts containing ionic Pt were activated by the reaction medium, while partial deactivation was observed for the prereduced ones. The activity improvement was associated with an increase in the ratio of Pt^{4+}/Pt^{2+} species on the surface of preoxidized catalysts. The activity decrease of the prereduced catalysts was due to the partial oxidation and subsequent redispersion of Pt particles. Introduction of H_2O and CO_2 to the reaction mixture only moderately influenced NH_3 oxidation activity shifting NH_3 conversion curves by about +15°C.

Introduction

Suppressing NO_x emissions from diesel engines is a challenge due to a lack of reducing agents in exhaust gas.[1] To solve this problem, the NH_3-SCR process (selective catalytic reduction of NO_x by ammonia), previously developed to remove NO_x from stationary sources, is effectively applied.[2] However, the excess of ammonia is used under NH_3-SCR conditions to maximize NO_x conversion which results in environment pollution by NH_3.[3] Integrated Heavy Duty Diesel (HDD) aftertreatment systems include diesel oxidation catalyst, catalyzed soot filter, NH_3-SCR component, and an ammonia slip catalyst (ASC), used to reduce ammonia emissions.[4] ASCs are also used to remove residual ammonia during the implementation of the $DeNO_x$ process, for example, in case of neutralization of NO_x produced by large utility boilers, industrial boilers, and municipal solid waste incinerators.[5] In this case, the use of the ASC catalyst should allow ammonia concentration in the exhaust gases of less than 10 ppm.[5]

The state-of-art ASC is a complex system comprising catalyst layers for ammonia oxidation (AMOX) and selective NO_x reduction (NH_3-SCR).[6] For the oxidation of ammonia, a Pt/Al_2O_3 catalyst is usually applied providing high low-temperature activity.[6b, 7] However, such a catalyst possesses relatively low N_2 selectivity due to the formation of N_2O at temperatures below 250°C and the formation of NO_x above 250°C.[7a, 8] To achieve maximal activity and reduce contribution from the by-products (N_2O, NO_x), it is necessary to establish factors governing the operation of Pt/Al_2O_3 during ammonia oxidation. At the same time it is important to reach the highest degree of Pt usage thus reducing the cost of aftertreatment systems.[9]

Activity and selectivity of the Pt/Al_2O_3 catalyst are affected by Pt dispersion because of the difference in the physicochemical properties of small and large Pt particles. For example, Pt metallic particles smaller than 3 nm exhibit semiconductor and dielectric properties due to the modification of electronic structure in comparison with bulk platinum.[10] Furthermore, the ratio of surface adsorption sites (vertices, edges, terraces) determining catalytic properties is different for small and large nanoparticles. In case of small particles, the fraction of surface atoms increases, while coordination numbers decrease.[10b] Note that tolerance towards reaction medium exposure (for example, excess of O_2) substantially depends on the initial size of platinum nanoparticles.

The strong influence of Pt crystallite size on catalytic properties of platinum catalysts in ammonia oxidation has been reliably established in the literature.[8, 11] It is known that small Pt particles exhibit lower activity compared to large crystallites. At the same time, N_2 selectivity increases with decreasing Pt particle size. In the available reports [8, 11a, 11b] only a narrow temperature range was studied, where NO and NO_2 were not formed. Besides, catalysts with different Pt content were compared. The catalytic data were obtained at high ratios of NH_3:O_2 (1:1 or 1:3, not relevant for exhaust aftertreatment) and/or at low temperatures under stationary conditions, which led to catalyst deactivation.[8b] Catalysts containing small Pt crystallites are most prone to deactivation due to oxidation of

platinum to PtO_x, where x depends on the crystallite size.[8b] Thus, there is a need to investigate in detail catalysts with different particle sizes of Pt, but with the same platinum content. Moreover, the catalytic measurements should be performed at low $NH_3:O_2$ ratios relevant for practical application over a wide temperature range. Note that under the conditions of diesel exhaust aftertreatment systems, it is important to study the effect of H_2O and CO_2 presence in reaction mixture.

The effect of Pt particles size on their catalytic properties in NH_3 oxidation in the temperature range of 150–550°C was studied under conditions relevant for diesel exhaust aftertreatment.[12] It was shown that an increase in the average Pt particle size from 1.3 to 18.7 nm was accompanied by a decrease in the T_{50} value from 233 to 215°C. With the increase of particle size to 200 nm, the T_{50} value decreased to ~200°C. The size effect on the yield of the main reaction products was negligible. A tendency to increase the N_2 yield and decrease the N_2O yield in case of large Pt particles was also shown. The influence of Pt particle size on the NO_2/NO_x ratio was found. The highest value of NO_2/NO_x ~ 0.65 was observed for particles with a size of 2.7 nm. The author concluded that it is possible to control the NO_2/NO_x ratio (important for the NH_3-SCR process) by varying the Pt particle size. For a catalyst exhibiting high N_2 selectivity, the most favorable ratio of $NO_2/NO_x = 0.5$ was achieved with a Pt particle size in the range of 2-8 nm.[6b] It should be noted that in work[12] the catalytic data were compared using NH_3 conversion curves measured during cooling in the reaction mixture. However, upon the first heating to 550°C, the initial state of the catalyst (including the particle size of Pt) could change significantly. A comparison of the curves of the 1st and 2nd heating/cooling cycles shows a significant decrease in the T_{50}

value for the most dispersed particles during the 2nd cycle. The authors do not discuss the reasons for this activation.

The aim of this work was to systematically study the effect of particle size and degree of Pt oxidation on the properties of Pt/Al_2O_3 catalysts in the reaction of ammonia oxidation under model ($NH_3 + O_2$/He mixture) and realistic conditions ($NH_3 + O_2 + CO_2 + H_2O/N_2$ mixture).

Results and Discussion

XRD data

X-ray diffraction patterns for all prepared catalysts and the γ-Al_2O_3 support are shown in Fig. S1a (see Supporting information). Samples N-Ox-400, Cl-Red-400, and the support show reflections of only the γ-Al_2O_3 phase (ICDD PDF-2 #29-0063), while reflections from Pt-containing compounds are not observed. This indicates a highly dispersed state of platinum species. In case of N-Ox-600, Cl-Red-550, Cl-Red-600 samples, in addition to the γ-Al_2O_3 phase, reflections from metallic Pt were observed (ICDD PDF-2 #04-0802). The sizes of Pt crystallites (determined by the Rietveld method) were 17, 2.2, and 6.4 nm for N-Ox-600, Cl-Red-550, Cl-Red-600 catalysts, respectively.

TEM data

According to TEM data, alumina support contains needle- and sheet-shaped γ-Al_2O_3 nanoparticles with d = 3-5 nm and l = 10-80 nm. Particles of γ-Al_2O_3 form porous crystalline aggregates with sizes of 50-300 nm.
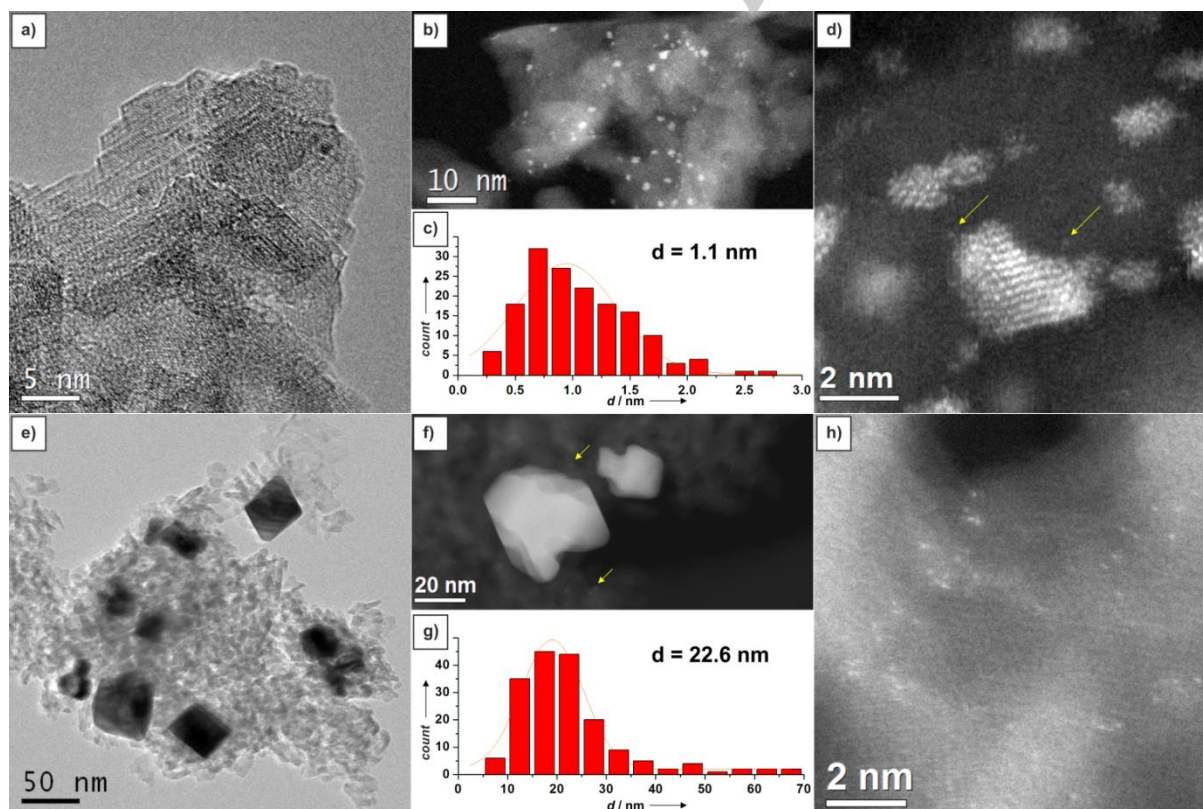
Figure 1. TEM micrographs for (a-d) N-Ox-400 and (e-h) N-Ox-600 catalysts: a, e - BF-TEM images; b, d, f, h - HAADF-STEM images; c, g - the Pt particle size distributions. Individual Pt atoms and small clusters with sizes less than 0.3 nm are marked with arrows.
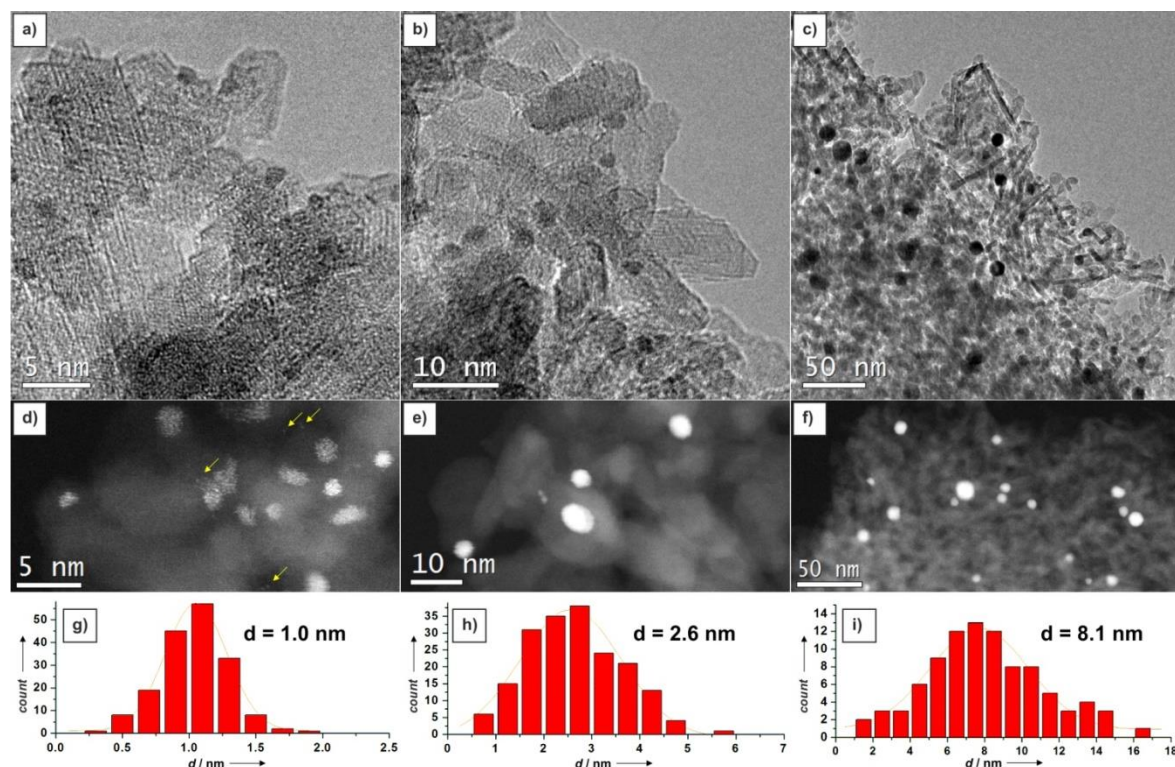
Figure 2. TEM micrographs for (a, d, g) Cl-Red-400, (b, e, h) Cl-Red-550 and (c, f, i) Cl-Red-600 catalysts: a-c - BF-TEM images; d-f - HAADF-STEM images; g-i - the Pt particle size distributions. Individual Pt atoms and small clusters with sizes less than 0.3 nm are marked with arrows.

Table 1. The XRD and TEM data on Pt particle sizes and Pt dispersion for all synthesized Pt/Al$_2$O$_3$ catalysts

Precursor	Treatment conditions			D(Pt), nm XRD	D(Pt), nm HRTEM	Dispersion HRTEM, %	Catalyst
	air/4h/T	H$_2$/2h/T	Ar/6h/T				
nitrate Pt	400°C	-	-	-	1.1	87.1	N-Ox-400
nitrate Pt	600°C	-	-	17 (1)	22.6	6.4	N-Ox-600
H$_2$PtCl$_6$	400°C	350°C	400°C	-	1.0	87.1	Cl-Red-400
H$_2$PtCl$_6$	400°C		550°C	2.2 (2)	2.6	46.9	Cl-Red-550
H$_2$PtCl$_6$	400°C		600°C	6.4 (3)	8.1	17.2	Cl-Red-600

In the N-Ox-400 catalyst, platinum nanoparticles are uniformly distributed over the support surface (Fig. 1a-d). The average Pt particle size is 1.1 nm (Fig. 1c). Note that the contribution of particles with sizes of less than 1 nm is quite large. In HAADF-STEM images (Fig. 1d) individual Pt atoms and small clusters with sizes less than 0.3 nm are detected (marked with arrows).

In case of the N-Ox-600 catalyst, larger platinum particles with an average size of 22.6 nm are observed (Fig. 1e-h). Such particles are characterized by isometric or irregular shape. The surface of well-crystallized particles is represented by extended {111} faces. After calcination at 600°C, highly-dispersed platinum species with the size less than 0.5 nm can still be detected in HAADF-STEM images (Fig. 1f, marked with arrows). Moreover, high-resolution HAADF-STEM imaging allowed us to detect single Pt atoms on alumina surface (Fig. 1h).

In the case of Cl-Red catalysts, spherical Pt nanoparticles are uniformly distributed over the entire support surface (Fig. 2a-c). Variation of calcination temperature in Ar allowed us to control the average particle size of Pt in Cl-Red samples. Cl-Red-400 sample contains Pt with the average size of 1.0 nm (Fig. 2g). Both nanoparticles and atomic Pt species are observed in the HAADF-STEM image (Fig. 2d). Argon calcination at 550°C leads to an increase in the average size to 2.6 nm (Cl-Red-550, Fig. 2h), while heating to 600°C - to 8.1 nm (Cl-Red-600, Fig. 2i). The number of observed highly dispersed Pt species decreases with the increase in the calcination temperature. Such species are not reliably detected in case of the Cl-Red-600 sample.

Quantitative XRD and TEM data for all studied samples are shown in Table 1. Thus, presented XRD and TEM data show that the used preparation methods allow synthesizing Pt/Al$_2$O$_3$ catalysts with a variation of the average Pt particle size in a wide range (from ~1 to ~25 nm). The presence of atomic Pt has also been revealed.

XPS data

3

Fig. 3 presents Pt4f spectra curve-fitted into the individual components (doublets) for all catalysts. The resulting $E_b(Pt4f_{7/2})$ values of the different platinum components and their contributions to the overall Pt4f spectra are given in Table 2.

The Pt4f spectrum of the N-Ox-400 sample can be fitted by two doublets with the $E_b(Pt4f_{7/2})$ values of 72.3 eV and 74.7 eV, which are typical for $Pt^{\delta+}/Pt^{2+}$ and Pt^{4+} species, respectively.[13] For the N-Ox-600 catalyst the main doublet is characterized by a maximum of $Pt4f_{7/2}$ peak at 71.5 eV. Such $E_b(Pt4f_{7/2})$ value is a bit higher than the one typical for bulk metallic Pt^0 ($E_b(Pt4f_{7/2})\sim71.1$ eV).[13a, 14] The shift to higher E_b values can be explained by formation of small metallic Pt^0 particles.[15] The second doublet component with $E_b(Pt4f_{7/2}) = 74.3$ eV can be attributed to Pt^{4+} species. Thus, the Pt4f spectra of the N-Ox catalysts show the presence of a substantial amount of oxidized Pt species.

In case of the Cl-Red catalysts the main state in the Pt4f spectra has an $E_b(Pt4f_{7/2})$ value of 71.4±0.1 eV which can be attributed to small Pt^0 particles. The doublet component with $E_b(Pt4f_{7/2}) \sim$ 74.1 eV typical for Pt^{4+} species is also observed but its intensity is very low. Contribution of the Pt^{4+} component to the overall Pt4f spectrum does not exceed 15%. Hence, XPS reveals more reduced Pt species in the case of the Cl-Red samples than in the N-Ox catalysts.

Quantitative evaluation of the XPS data were performed to demonstrate different Pt_{at}/Al_{at} ratios obtained for the N-Ox and Cl-Red catalysts (see Table 2) with the same Pt loading. Pt_{at}/Al_{at} ratios in the N-Ox samples are at least 2 times higher than the ones in the Cl-Red samples. Probably, the oxidative pretreatment (in 20%O_2/He) induces formation of highly dispersed Pt species on the Al_2O_3 surface in the N-Ox samples. Calcination of the N-Ox sample at 600°C might also induce sintering of Pt particles due to high volatility of PtO_2 species resulting in Ostwald ripening. As a result, the Pt_{at}/Al_{at} ratio decreases in comparison with the N-Ox-400 catalyst. The TEM data for the N-Ox-600 catalyst reveal appearance of Pt nanoparticles with the average size of 22.6 nm. However, highly dispersed Pt species can still be observed (Fig. 1 f, h), explaining quite high Pt_{at}/Al_{at} ratio of 0.6. Based on the comparison of Pt_{at}/Al_{at} values between Cl-Red and N-Ox catalysts it can be concluded that calcination in Ar decreases the number of highly dispersed Pt species. It results in the decreased intensity of the Pt4f signal. Low Pt_{at}/Al_{at} ratios for Cl-Red-550 and Cl-Red-600 catalysts in contrast to Cl-Red-400 sample might also be caused by Pt sintering in agreement with the XRD and HRTEM data.
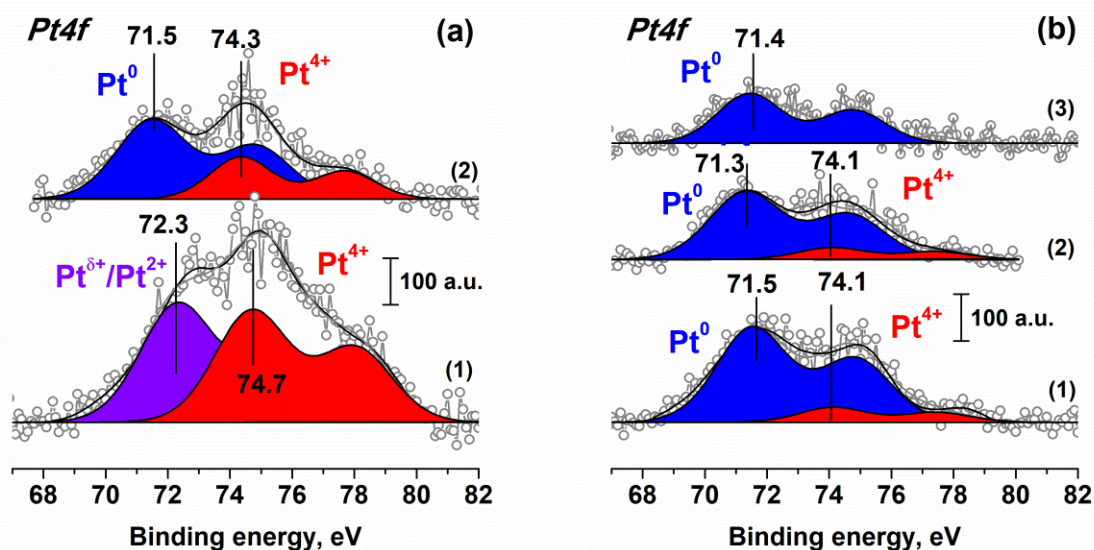

Figure 3. Pt4f spectra of (a) the N-Ox catalysts: (1) N-Ox-400 (PtOx, 1.1 nm), (2) N-Ox-600 (Pt^0, 22.6 nm); (b) the Cl-Red catalysts: (1) Cl-Red-400 (Pt^0, 1.0 nm), (2) Cl-Red-550 (Pt^0, 2.6 nm); (3) Cl-Red-600 (Pt^0, 8.1 nm). (Pt4f spectra of all samples were normalized to the common Al2p intensity).

Table 2. XPS data: Pt_{at}/Al_{at} ratio, $E_b(Pt4f_{7/2})$ values of the different Pt components and their contribution to the overall Pt4f spectrum.

Sample	Pt_{at}/Al_{at}, %	$E_b(Pt4f_{7/2})$			$I(Pt^o)$, %	$I(Pt^{\delta+}/Pt^{2+})$, %	$I(Pt^{4+})$, %
		Pt^o	$Pt^{\delta+}/Pt^{2+}$	Pt^{4+}			
N-Ox-400	1.0	-	72.3	74.7	-	50	50
N-Ox-600	0.6	71.5	-	74.3	70	-	30
Cl-Red-400	0.5	71.5	-	74.1	90	-	10
Cl-Red-550	0.4	71.2	-	73.5	80	-	20
Cl-Red-600	0.2	71.4	-	-	100	-	-

4

Catalytic properties in the NH₃ oxidation (model mixture)

Fig. 4a presents NH₃ conversion curves for N-Ox catalysts with different air-calcination temperatures. The curves were measured during the first and the second heating in the model reaction mixture (1000ppm NH₃, 4% O₂, He, GHSV=120,000 h⁻¹). At low temperatures (<150°C), the apparent NH₃ conversion is negative due to NH₃ desorption during heating. The high adsorption capacity of Al_2O_3-based catalysts was discussed in our previous work.[16] Temperature of 50% NH₃ conversion (T_{50}) for the N-Ox-400 catalyst is ca. 237°C, while for N-Ox-600 there is a noticeable increase in activity (T_{50} ~ 160°C). After the first heating-cooling cycle in the reaction mixture the N-Ox-400 sample becomes more active (NH₃ conversion curve shifts by 5°C towards low temperatures, T_{50} = 232°C) and the N-Ox-600 catalyst slightly deactivates (the conversion curve shifts by 15°C towards high temperatures, T_{50} ~ 175°C).

The highest N₂ concentration is detected at ~270 and ~170°C for the N-Ox-400 and N-Ox-600 catalysts, respectively (Fig. 4b). N₂O concentration profile over the N-Ox-600 catalyst (Fig. 4d) shows two maxima at ~175 and ~260°C. For the N-Ox-400 catalyst, only one N₂O concentration maximum is observed at about 260°C. Fig. 4c presents N₂ selectivity (S_{N2}) data for N-Ox-400 and N-Ox-600 catalysts. The maximal S_{N2} for the N-Ox-400 catalyst is higher (90%) than for the N-Ox-600 (80%). The difference is caused by the N₂O release below 200°C from the N-Ox-600 sample (Fig. S2). N₂ selectivity decreases with increasing temperature and becomes similar for both N-Ox-400 and N-Ox-600 catalysts above 315°C. At the same time NO$_x$ is detected at temperatures above 225-275°C (Fig. S3) leading to decreased selectivities to N₂ and N₂O. Note that the difference in S_{N2} values measured during the 1st and 2nd heating is negligible (Fig. 4c).

Fig. S4 presents amount of reaction products per nitrogen atoms depending on temperature. Upon reaching 100% NH₃ conversion, the amount of N-containing products for the N-Ox-600 catalyst is 30% higher than the concentration of NH₃ in the feed. It might be related to the increased amount of NH₃ adsorbed by the catalyst during its pretreatment in the reaction mixture at room temperature. During the subsequent heating, part of the adsorbed NH₃ can be converted to N₂ and N₂O, providing their overstoichiometric amounts at the outlet of the reactor. For the N-Ox-400 catalyst, the amount of the released reaction products is practically equal to the initial concentration of NH₃.
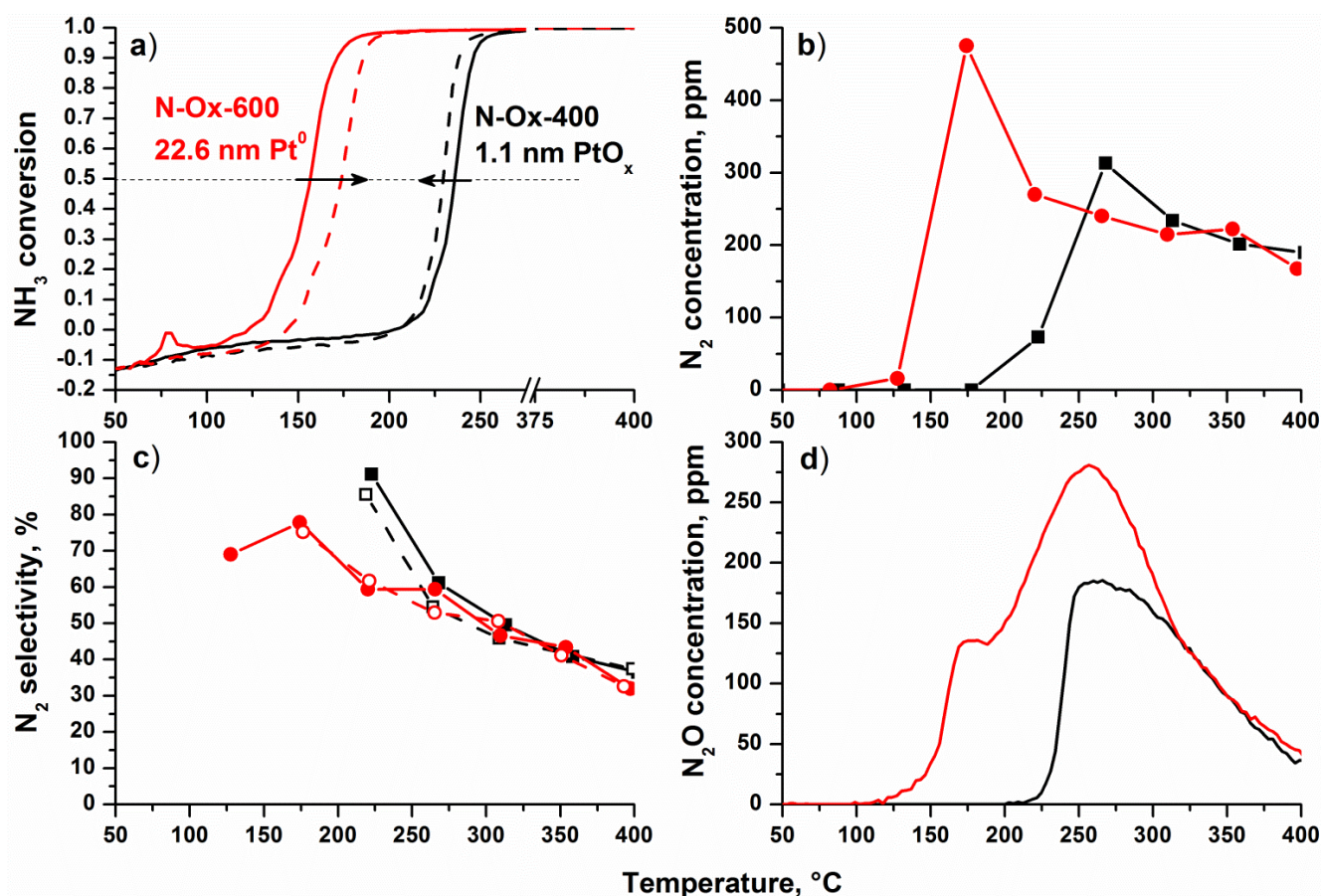

Figure 4. a) – NH₃ conversion curves, b) and d) – N₂ and N₂O concentrations respectively, c) – N₂ selectivity for N-Ox-400 (black lines) and N-Ox-600 catalysts (red lines). Data collected during the first (solid lines, closed symbol) and the second (dashed lines, open symbol) heating in the reaction mixture.

Fig. 5 gives a comparison of the catalytic data for catalysts with similar Pt dispersion but different degrees of Pt oxidation (N-Ox-400 and Cl-Red-400). T_{50} values measured during the first heating of N-Ox-400 and Cl-Red-400 catalysts are 237 and 180°C, respectively. During the second heating, shifts of the NH₃ conversion curves by ~5-10°C, towards lower (for N-Ox-400) and higher (for Cl-Red-400) temperatures, are observed. Taking into account the XPS data (Fig. 3) and the similar Pt dispersion for the N-Ox-400 and Cl-Red-400 samples (Table 1), it can be concluded that Pt⁰ metallic particles on the Al_2O_3 surface

demonstrate significantly higher activity in the ammonia oxidation reaction than oxidized PtO_x species. Note that the XPS data show that Pt/Al ratio (table 2) in the N-Ox-400 catalyst is two times higher than in the Cl-Red-400 catalyst, indicating a higher number of Pt sites. However, this increase in the number of Pt sites did not lead to an increase in catalytic activity. This is due to the large fraction of atomically dispersed oxidized PtO_x species, which are not visible in HRTEM of the N-Ox-400 catalyst and have low activity.

N_2 and N_2O concentration curves are similar for the N-Ox-400 and Cl-Red-400 catalysts above 250°C (Fig. 5b, d), while significant differences are observed below 250°C. In case of the Cl-Red-400 sample, N_2 and N_2O are first detected at lower temperatures than for the N-Ox-400 catalyst. Note that the N_2 and N_2O concentration curves for Cl-Red-400 have additional peaks in the temperature range 180-230°C. The appearance of these narrow peaks (similar to the data from Fig. S2) might be associated with two reasons. The first reason is related with desorption of overstoichiometric amounts of reaction products formed due to NH_3 adsorption at low temperatures at the Pt surface. The second one can be related to the reaction of NH_3 desorbing from the alumina support (see exemplary NH_3-TPD profile in Fig. S5).

The calculated S_{N2} values are shown in Fig. 5c. At NH_3 conversions of less than 100%, the S_{N2} values reach 90% and 80% for the pre-oxidized N-Ox-400 and the pre-reduced Cl-Red-400 catalysts, respectively. At 100% NH_3 conversion (above 270°C), the S_{N2} values decrease for both catalysts to ~40%. The S_{N2} curves measured during the 1st and 2nd heating are similar. NO_x formation is observed at temperatures above 250°C (Fig. S6a). The NO_2/NO_x ratio at T <375°C is significantly higher for the Cl-Red-400 sample than for the N-Ox-400 catalyst (Fig. S6b). This ratio reaches ~0.7 for Cl-Red-400, indicating the predominant formation of NO_2 on the surface of metallic platinum.

Catalytic properties of the Cl-Red catalysts containing metallic Pt particles of various sizes are compared in Fig. 6. The T_{50} values for Cl-Red-400, Cl-Red-550, and Cl-Red-600 catalysts during the first heating (Fig. 6a) are ~180, 165, and 155°C, respectively. During the second heating, the T_{50} value remains unchanged for the Cl-Red-550 catalyst, while in case of Cl-Red-400 and Cl-Red-600 the NH_3 conversion curves are shifted towards high temperatures reaching the T_{50} value of 190 and 165°C, respectively. In a similar way, for the N-Ox-600 catalyst containing large metallic Pt particles (22.6 nm), the T_{50} increases from 160 to 175°C between the first and second heating curves.
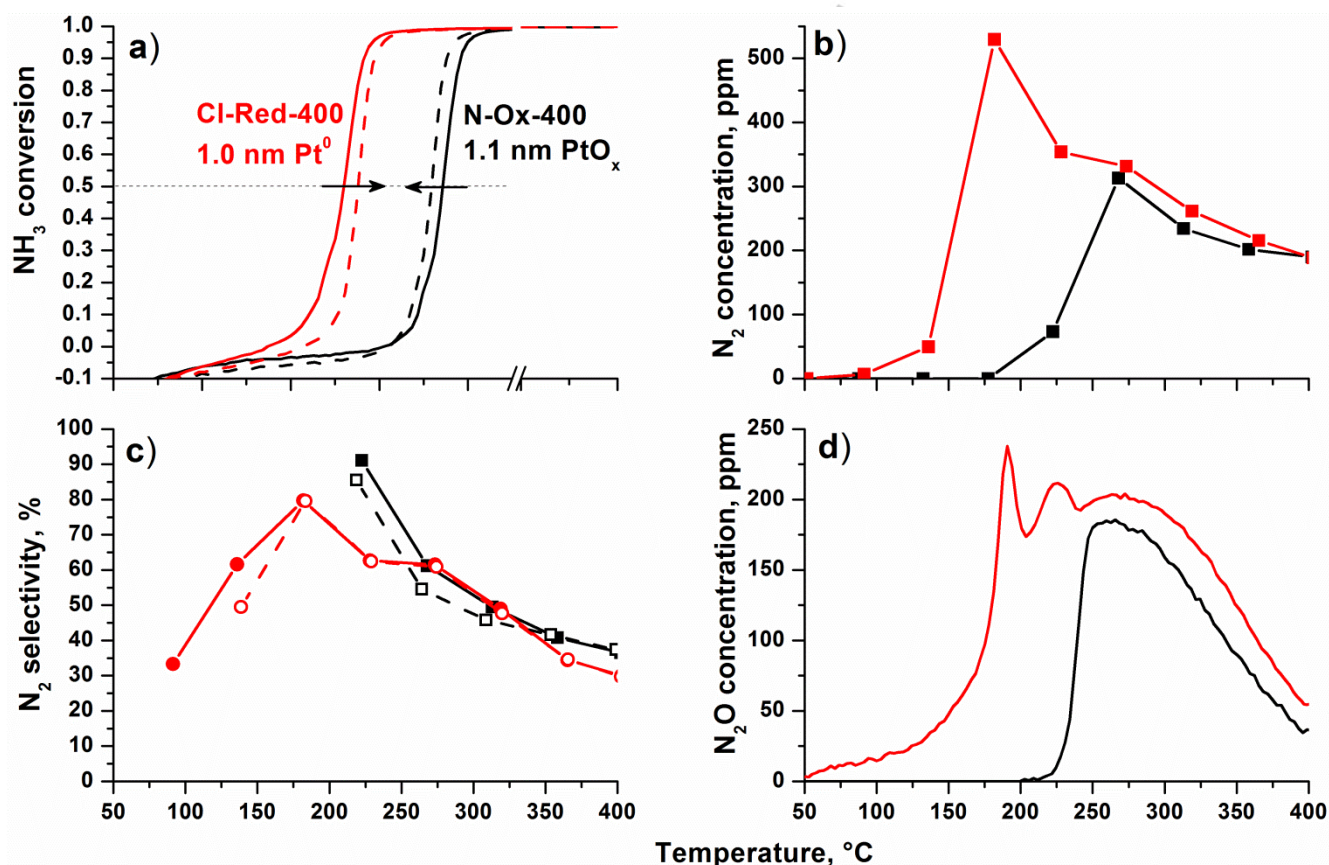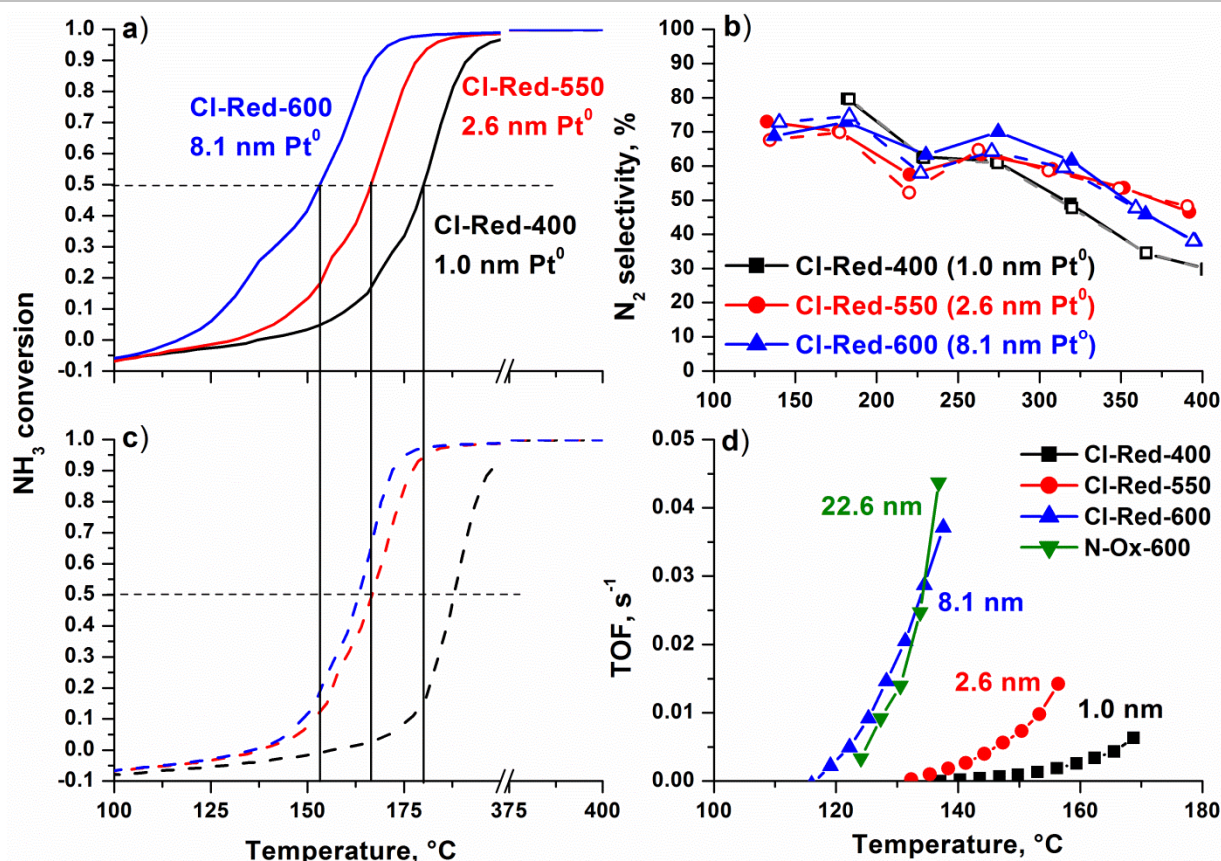

Figure 5. a) NH_3 conversion curves, b) N_2 and d) N_2O concentration, and c) N_2 selectivity for N-Ox-400 (black lines) and Cl-Red-400 (red lines) catalysts. Data collected during the first (solid lines, closed symbol) and the second (dashed lines, open symbol) heating in the reaction mixture.

Figure 6. (a, c) NH$_3$ conversion curves obtained over Cl-Red catalysts during a) the first (solid lines) and c) second (dashed lines) heating in the reaction mixture. Vertical lines in Fig. 6a, c correspond to the T$_{50}$ values for the first heating curves. (b) N$_2$ selectivity during the first (solid lines, closed symbol) and the second (dashed lines, open symbol) heating of the catalysts in the reaction mixture. (d) A plot of TOF versus temperature during the first heating of Cl-Red-400, Cl-Red-550, Cl-Red-600, and N-Ox-600 catalysts.

The N$_2$ and N$_2$O concentration curves for Cl-Red catalysts are shown in Fig. S7. The N$_2$O and N$_2$ curves show two maxima, this becomes clearer when N$_2$ profiles calculated from the FTIR data are analyzed (Fig. S8). N$_2$ selectivity is mainly determined by the reaction temperature, with the minor influence of the size of Pt particles or the pretreatment conditions (Fig. 6b). At higher temperature (>250°C), N$_2$O concentration decreases leading to an increase in S$_{N2}$ to 60-70%. A further increase in temperature leads to a decrease in S$_{N2}$ to 30-45% and increase of the contribution from NO$_x$ (Fig. S9a). Above 325°C, the S$_{N2}$ value is lower for Pt particles of about 1 nm (Cl-Red-400) due to the increased contribution from NO$_x$ (Fig. S9a). The NO$_2$/NOx ratio is almost independent of the metallic Pt particle size and limited by thermodynamic equilibrium (Fig. S9b).

Figure 6d shows TOF values calculated for the first heating curves taking into account Pt dispersion. These data show that lowering Pt dispersion leads to a sharp increase in the rate of ammonia oxidation. For instance, an increase in Pt sizes from 2.6 nm (Cl-Red-550) to 8.1 nm (Cl-Red-600) is accompanied by an increase in the TOF value by 30 times (at 140°C) at similar activation energies of 42 and 45 kcal/mol, accordingly (the corresponding Arrhenius plots are presented in Fig. S10).

Investigation of the catalysts after reaction by XPS and TEM

To shed light on the reasons for different activity during the first and the second heating in the NH$_3$ + O$_2$ mixture, the catalysts after reaction (denoted as AR = after reaction) were analyzed by HRTEM and XPS (Fig. 7, S11).

The size of Pt particles for the N-Ox-400 sample changes only slightly after catalysis. A large number of atomically dispersed Pt species is observed in the N-Ox-400-AR sample with a predominance of subnanometer particles. The average particle size is decreased to 0.8 nm while the overall range of particle sizes is maintained after catalysis testing (Figs. 1c and 7c).

A bimodal Pt particle size distribution is observed for the N-Ox-600-AR catalyst (Fig. 7d). Pt particle faceting becomes less rough due to truncation of sharp angles between the {111} planes. The sample contains many particles with round and irregular shapes. In addition to large particles with an average size of 17.5 nm, a lot of particles with an average size of 1.4 nm are observed (inset in Fig. 7d). Note that the initial N-Ox-600 sample contained some subnanometer Pt and atomic Pt species fixed on the support surface (Fig. 1g). Apparently, during the catalytic reaction these species grow in size due to the transfer of platinum from the surface of large crystalline particles. This leads to a decrease in the average platinum particle size in the N-Ox-600-AR catalyst compared to the as-synthesized sample.
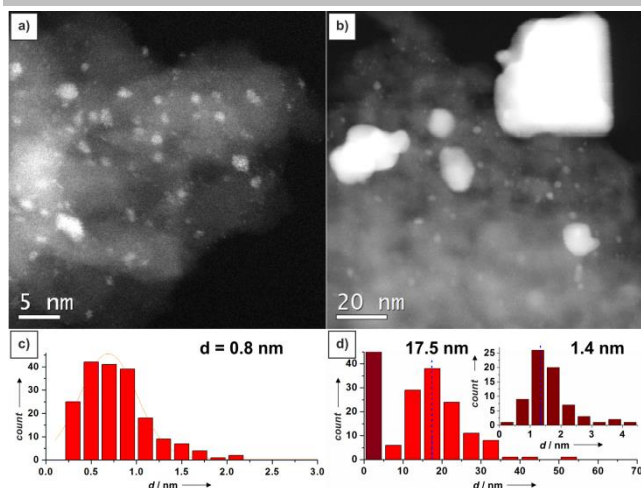
Figure 7. (a-b) HAADF-STEM images and (c-d) the diagrams of Pt particle size distribution for used (a, c) N-Ox-400-AR, (b, d) N-Ox-600-AR catalysts. Inset in Fig. 7d shows Pt particle size distribution in the narrow range of 1-4 nm.

On the contrary, in the Cl-Red-400 catalyst a slight enlargement of platinum nanoparticles from 1.0 to 1.3 nm occurs under reaction conditions (see Figs. 2g and 8d). The atomically dispersed Pt species in case of the Cl-Red-400 are preserved after catalytic tests. However, the particle size distribution broadens up to 4 nm. Such broadening of the particle size distribution may occur due to Ostwald ripening. At elevated temperature and high O_2 concentration volatile PtO_2 species are formed.[17] The transfer of such species to the surface of platinum or Al_2O_3 support leads to growth of existing Pt particles or appearance of additional highly dispersed species.

A similar process takes place in other Cl-Red samples. According to TEM (Fig. 8), a slight increase in the average particle size (from 2.6 nm to 3.0 nm) is observed in the Cl-Red-550 catalyst after reaction. On the contrary, in the Cl-Red-600-AR the calculated average particle size decreases from 8.1 nm to 7.0 nm. Apparently, the resulting change in the Pt size is determined by the transfer of PtO_x to the surface of other platinum particles or to the defects on alumina surface. This, in turn, directly depends on the initial size of platinum nanoparticles and the number of highly-dispersed platinum species on the surface which can act as seeds for growing nanoparticles.
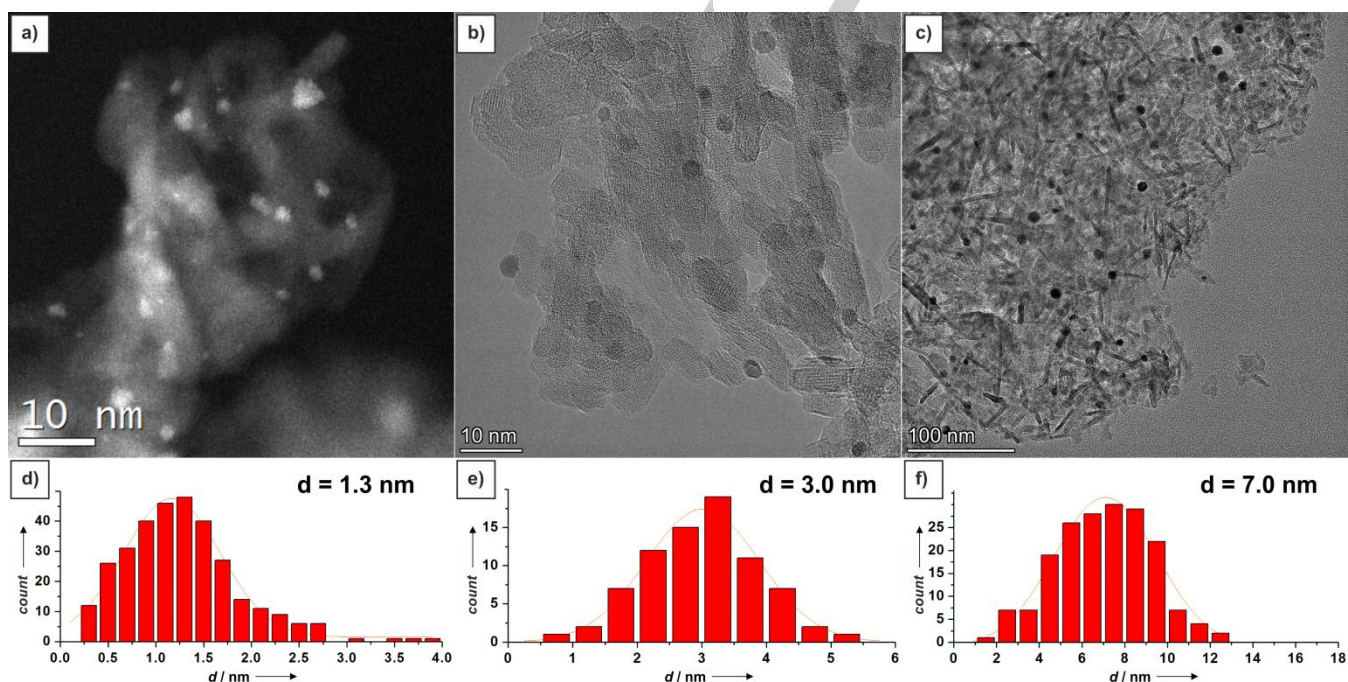
Figure 8. (a-c) HAADF-STEM images and (d-f) the diagrams of Pt particle size distribution for used (a, d) Cl-Red-400-AR, (b, e) Cl-Red-550-AR and (c, f) Cl-Red-600-AR catalysts.

Table 3. XPS data for the pristine and used catalysts: Pt_{at}/Al_{at} ratio, the $E_b(Pt4f_{7/2})$ values of the different Pt components and their contribution to the overall Pt4f spectrum.

Sample	Pt_{at}/Al_{at}, %	$E_b(Pt4f_{7/2})$			$I(Pt^o)$, %	$I(Pt^{\delta+}/Pt^{2+})$, %	$I(Pt^{4+})$, %
		Pt^o	$Pt^{\delta+}/Pt^{2+}$	Pt^{4+}			
N-Ox-400	1.0	-	72.3	74.7	-	50	50
N-Ox-400-AR*	0.9	-	72.5	74.6	-	45	55
N-Ox-600	0.6	71.5	-	74.3	70	-	30

8

N-Ox-600-AR	0.4	71.5	-	74.4	75	-	25
Cl-Red-400	0.5	71.5	-	74.1	85	-	15
Cl-Red-400-AR	0.6	71.6		73.7	80	-	20
Cl-Red-550	0.4	71.3	-	74.1	85	-	15
Cl-Red-550-AR	0.5	71.3		74.4	90	-	10
Cl-Red-600	0.2	71.4	-	-	100	-	-
Cl-Red-600-AR	0.2	71.1	-	74.1	90	-	10

*AR – after catalytic reaction of NH_3 oxidation (data is presented in Figs.4-6)

The Pt4f spectra of the catalysts after reaction are presented in Fig. S11. Note that after the second heating in the reaction medium, the catalysts were cooled to room temperature in He. XPS data on the surface Pt content (given as Pt_{at}/Al_{at} ratio) and the amount of various platinum states for the pristine and used catalysts are presented in Table 3. In case of the N-Ox-400 sample, a slight decrease in the amount of $Pt^{\delta+}/Pt^{2+}$ and corresponding growth of the contribution from the Pt^{4+} takes place after the catalytic tests. For the N-Ox-600 sample, an increase in the amount of the reduced Pt^o species is observed for N-Ox-600-AR. The surface platinum content for N-Ox catalysts decreases slightly after reaction. In accordance with TEM data, for N-Ox-600 sample it might be explained by the decrease of the number of the atomically dispersed Pt species during the reaction (Figs.1 and 7).

For the Cl-Red-400-AR sample an increase in the contribution of the oxidized Pt^{4+} species from 15 to 20% is observed. TEM data show an increase in the amount of highly dispersed (<1 nm) Pt species for this sample (Fig.8). Such species can be easily oxidized to Pt^{4+} upon exposure to O_2. Pt^{4+} can be additionally formed as a result of oxidation of the surface of metallic particles. Also for the Cl-Red-600 catalyst appearance of the Pt^{4+} on the surface (~10% contribution, Table 3) is revealed by XPS. Hence, partial oxidation of Pt to the Pt^{4+} state during the reaction can be proposed. For the Cl-Red-550 sample before and after catalytic measurements, quantitative distributions of platinum species are similar. The Pt_{at}/Al_{at} ratios for the Cl-Red samples increase after catalysis which may indicate higher Pt dispersion.

Catalytic properties in the NH_3 oxidation (realistic mixture)

N-Ox-400 and Cl-Red-400 catalysts with similar average size of Pt particles (~1 nm) but different oxidation state of Pt, as well as the Cl-Red-600 catalyst containing large metallic Pt particles (8.1 nm) were selected for additional tests in the realistic catalytic mixture containing CO_2 and H_2O (500ppm NH_3, 13% O_2, 5%H_2O, and 10%CO_2 in N_2, GHSV=600,000 h^{-1}). H_2O and CO_2 were added to the reaction mixture at 50°C after two heating – cooling cycles in NH_3+O_2 atmosphere before the third catalytic run.

Figure 9a-c shows NH_3 conversion and N_2 selectivity curves obtained during three consecutive heating-cooling cycles in the model (1st and 2nd cycles) and realistic (3rd cycle) reaction mixtures at high GHSV=600,000 h^{-1}. In the case of the N-Ox-400 catalyst, activation is observed after the 1st cycle (T_{50} decreases from 275 to 250°C), while deactivation takes place for Cl-Red-400 and Cl-Red-600 catalysts (T_{50} values increase from 230 and 190°C to 235 and 207°C, respectively). The data are completely consistent with the results obtained in the model mixture at lower GHSV. During the third heating in the realistic reaction mixture, an increase in T_{50} by 10-15°C is observed for all studied catalysts. Thus, introduction of CO_2 and H_2O into the reaction mixture leads to a moderate inhibition of NH_3 oxidation. Additional tests with adding only H_2O or CO_2 to the gas feed (not shown) suggest that the effect can be attributed to water addition. Figure 9d-f presents the selectivities to different products versus temperature for three successive heating runs in the reaction mixture. Selectivity is calculated using the data presented in Fig. S14-S16. Addition of water only slightly affects selectivities by increasing S_{N2O} and decreasing S_{N2} at medium temperatures. As demonstrated by Shrestha et al., water is not directly accounted for in the kinetic model of ammonia oxidation.[18] However, water is known to compete for ammonia adsorption sites on acidic supports [19] in this way diminishing the NH_3 surface coverage (θ_{NH3}) [20] and slowing down N_{ads} intermediate formation. On the other hand, water does hinder oxygen activation on the most common Pt surfaces at ASC operation temperatures [21] leading to lower N_{ads}/O_{ads} ratio and resulting in higher S_{N2O} in the medium temperature range. At higher temperatures (T>250°C) water effect on NH_3 adsorption on the catalysts is low [19a] and no effect on the reaction is observed (equally high S_{NOx} are observed).

Discussion

A study of Pt/Al_2O_3 ammonia slip catalysts was carried out using a combination of structural and spectral techniques. Prepared catalysts contained metallic or oxidized Pt particles with varied Pt dispersion. The effects of catalyst pretreatment, Pt particle size, and the exposure to the reaction mixture on the activity and selectivity of Pt/Al_2O_3 catalysts in ammonia oxidation are discussed below.

Effect of the catalyst pretreatment

According to the TEM (Figs. 1 and 2) and XPS (Fig. 3) data, calcination in air at 400°C leads to the formation of oxidized ~1 nm PtO_x particles. Such PtO_x particles can be reduced by H_2 in the temperature range of 40-140°C.[22] The preoxidized Pt/Al_2O_3 catalyst shows low activity in ammonia oxidation (T_{50} value ~240°C). Calcination of this catalyst in air at 600°C results in sintering of Pt with the formation of metallic Pt particles with an average size of 22.6 nm (Fig.2) in line with the previous reports.[23] An increase in Pt particle size simultaneously with the Pt reduction leads to a significant activation of the catalyst (T_{50} decreases to 175°C, Fig. 4).

Also the catalysts reduced in H_2 were prepared and studied after pretreatment in inert atmosphere. The use of H_2PtCl_6 as a

precursor allowed preserving the Pt dispersion during the subsequent reduction treatment,[16] while use of platinum nitrate as a precursor leads to a bimodal distribution of Pt particles with sizes of about 1 and 2 nm.[24] XPS data show different platinum states in the preoxidized (N-Ox-400) and prereduced (Cl-Red-

400) catalysts (Fig. 3) with similar Pt dispersion (Figs. 1 and 2). In case of the prereduced catalyst, metallic Pt is the main state (~87%), while the contribution of oxidized species (Pt^{4+}) is close to 13%. A combination of $Pt^{\delta+}/Pt^{2+}$ and Pt^{4+} species is found on the surface of the preoxidized catalyst.
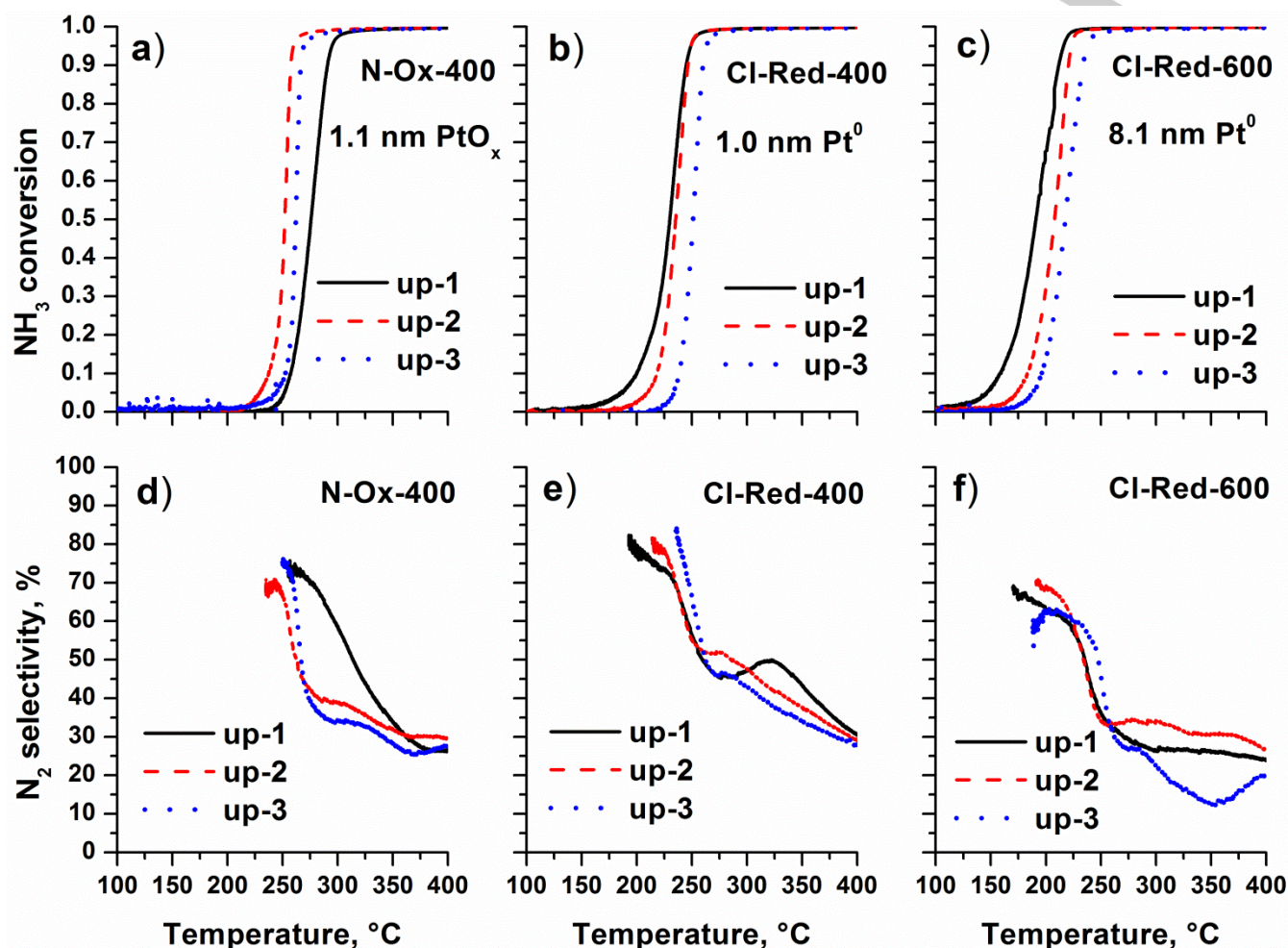

Figure 9. NH$_3$ conversion and N$_2$ selectivity curves for N-Ox-400, Cl-Red-400 and Cl-Red-600 catalysts obtained during three consecutive heating in model (Up-1, Up-2) and realistic (Up-3) a reaction mixture.

The catalytic activity of the prereduced Pt/Al$_2$O$_3$ catalyst is significantly higher than the activity of the preoxidized one with the difference in the T_{50} values ΔT_{50}~55°C (Fig.5). Therefore, it can be reliably concluded that for samples with similar Pt dispersion metallic Pt^0 species demonstrate improved activity in NH$_3$ oxidation in comparison with PtO_x species. This conclusion is in agreement with literature data.[25] The increased activity is associated with the formation of reactive intermediate NH$_x$ species as a result of breaking of N-H bonds during the oxidative ammonia dehydrogenation on metallic surface. This process proceeds efficiently with the participation of atomic oxygen formed by the O$_2$ dissociation. It was established that adsorbed oxygen on the surface of Pt plays the main role in the mechanism of the oxidative ammonia dehydrogenation. The activation of NH$_3$ molecule proceeds much more efficiently on the surface of metallic platinum than on the oxidized Pt.[11b, 25a] We also note that the mechanism of NH$_3$ oxidation over oxidized clusters and PtO$_x$ nanoparticles may differ from that for metallic platinum.[26] This assumption is confirmed by a significant

difference (>50°C, Fig. 5) in the onset temperature of ammonia oxidation reaction on preoxidized and prereduced catalysts.

Effect of Pt particle size

Pt/Al$_2$O$_3$ catalysts with different Pt dispersion were prepared (average particle sizes of ~1, ~2.5, and ~8, Fig. 2). To control the particle size of Pt, the prereduced catalyst was calcined in inert atmosphere at different temperatures. According to the XRD and TEM data, calcination in Ar at 550-600°C leads to the transition of platinum from the atomically dispersed to the nanoscale state (Fig. 2 and Table 1), while the charge state of platinum changes negligibly (XPS data, Fig. 3). Note that in the case of the preoxidized catalyst, calcination in air at 600°C results in the growth of Pt particles and reduction of platinum (Figs. 1 and 3). The influence of both factors ensures evident activation of the catalyst (a decrease in the T_{50} value by 77°C, Fig. 4), while an increase in the size of metallic Pt particles is accompanied by a shift of the NH$_3$ conversion curve towards lower temperatures by only ~25°C (Fig. 6).

The most active Pt/Al_2O_3 catalysts contain crystalline Pt^0 particles with average sizes of ~8 and ~23 nm. Such catalysts display similar T_{50} values. This indicates that the most significant changes in activity take place when the Pt particle size changes from ~1 to ~8 nm.

The low activity of the catalysts containing highly dispersed metallic Pt is associated with the facile formation of PtO_2 species directly under reaction conditions.[27] The appearance of such species hinders activation of O_2, in contrast to crystalline Pt^0 nanoparticles. In the latter case, only a thin surface PtO_x layer is formed. It was found that chemisorbed oxygen on the surface of metallic Pt shows significantly higher catalytic activity than oxygen from the bulk platinum oxide.[27-28]

An increase in the size of Pt nanoparticles from ~1 to ~8 nm leads to an increase in the number of platinum atoms with a high coordination number, ensuring appearance of terraces on the surface. A change in the particle size from 2.5 to 4.2 nm is accompanied by the increase in the amount of terrace-like sites by 50%.[29] Moreover, the largest changes in the number of terraces on the surface of Pt nanoparticles take place in the size range from ~2 to ~3 nm. Further growth of Pt particles leads to an increase in the degree of crystallinity with the appearance of isometric crystal faceting due to the development of {111} faces. Such behavior is observed for the Pt/Al_2O_3 catalyst calcined at 600°C (Figs.1e-f).

An increase in catalytic activity along with the growth of Pt^0 crystallites can be related to the effective activation of O_2 on platinum terraces.[30] In case of the highly dispersed platinum, strong oxygen adsorption on coordinatively unsaturated sites (edges, kinks, corners etc.) facilitates the formation of PtO_x species.[31] Niwa et al.[32] and Briot et al. [33] demonstrated that weakly bound oxygen on the catalyst surface provides higher activity and the reactivity of chemisorbed oxygen increases with the growth of Pt^0 particles.

A similar relationship between Pt^0 crystal size and the catalytic activity was observed in benzene oxidation over Pt/Al_2O_3 occurring in the same temperature range (25-400°C) [34]. It was established that the number of Pt-O bonds with lower binding energy (or higher oxygen reactivity) was greater for large Pt particles. Additionally, 2–3 nm Pt particles with the largest contribution of surface atoms (with low coordination numbers) were found to be the most active in the oxidation of CO under lean conditions.[11c] Moreover, oxidation of NO occurred more efficiently on large particles with predominant extended facets.

It is known that TOF increases with the growth of Pt particle size due to effective dissociation of O_2 with the formation of reactive oxygen species on large particles.[8a] This was confirmed by our results, according to which an increase in Pt particle size from 2.6 to 8.1 nm leads to an increase in the TOF value by 30 times (Fig.6d). Note that further particle growth to 22.6 nm does not change TOF.

Effect of the reaction mixture

For each catalyst two (or three) heating-cooling cycles in the reaction mixture were carried out during catalytic tests. In case of the Pt/Al_2O_3 catalyst with large Pt^0 particles (~22.6 nm, Fig. 1g), a decrease in activity is observed during the second heating (the conversion curve shifts towards higher temperatures, Fig. 4). This is accompanied by an increase in Pt dispersion and a change in faceting of Pt particles, leading to a decrease in the number of terrace sites and truncation of sharp angles between {111} faces (TEM data, Fig. 7).

In case of the highly dispersed (~1 nm) PtO_x particles on the surface of the preoxidized Pt/Al_2O_3 catalyst, a slight improvement in activity takes place after exposure to the reaction medium (Fig. 4). The reduction of the oxidized Pt species during the reaction might result in the improvement of the activity. However, XPS data reveal only Pt^{4+} and Pt^{2+} species on the surface of the sample after reaction without appearance of metallic Pt^0 (Fig. S10, Table 3). We can propose that reduced Pt species formed during the reaction are reoxidized upon contact of the sample with O_2. The presence of only ionic Pt^{4+} and Pt^{2+} species confirms preservation of the highly dispersed platinum particles during the reaction.

In contrast to the preoxidized PtO_x/Al_2O_3 samples, the prereduced Pt^0/Al_2O_3 catalysts with platinum particle sizes of ~1 and ~8 nm are deactivated during catalytic tests (Fig. 6). For Pt^0 particles with a size of ~1 nm, an increase in the number of Pt^{4+} sites is observed after the reaction (Table 3). The appearance of Pt^{4+} species after catalytic tests is also observed for platinum particles of ~8.1 nm (Table 3). Thus, the deactivation of prereduced catalysts correlates with an increase in the contribution of Pt^{4+} species, which are significantly less active than metallic Pt. The decrease in the activity of Pt catalysts can be related to the effective formation of PtO_2 species during the reaction.[8b] Such species are formed as a result of the local overheating of the catalyst grain due to the exothermic effect of the oxidation reaction but easy oxidation of undercoordinated Pt sites.

It may be concluded that the growth of the Pt^{4+} surface content is accompanied by a decrease in the contribution of metallic Pt, which activates O_2 and NH_3. This results in the drop of the NH_3 oxidation activity. The catalytic activity of the prereduced Pt/Al_2O_3 sample with Pt^0 particles of ~2.6 nm remains unchanged due to the preservation of Pt surface state. The appearance of small PtO_x species, as well as efficient oxidation of Pt surface might be considered as the main reason for the deactivation of Pt supported catalysts in NH_3 oxidation.

Effect of Pt dispersion and Pt state on selectivity in the NH_3 oxidation

For the preoxidized and prereduced Pt/Al_2O_3 catalysts with similar Pt dispersion (~1 nm), the N_2 and N_2O concentration profiles are clearly different (Fig. 5). In case of the prereduced sample, the N_2/N_2O concentration curves show additional narrow low-temperature peaks at T<250°C, while for the preoxidized catalyst, the corresponding curves contain one wide peak. Low-temperature peaks are presumably associated with the removal of N, NH_x, NO intermediate species that may inhibit O_2 adsorption. Indeed, the platinum surface was found to be deactivated at low temperatures due to the formation of strongly bonded N, NH_x, NO and OH species.[5, 35] Atomic oxygen reacts with NH_x species to form OH groups,[25a, 25b, 26, 36] which are formed after abstraction of all H atoms from the adsorbed NH_3 molecule.[35] Molecular nitrogen is formed as a result of recombination of N_{ad} (ad = adsorbed) species, while the interaction of N_{ad} and O_{ad} leads to the appearance of NO_{ad}.[35] An increase in temperature removes adsorbed oxygen and NH_x species with the formation of N_2 and N_2O products (Fig. 4, 5, S7 and S8). The ratio of N_{ad} and NO_{ad} species depends on the reaction temperature. N_{ad} species prevail on the platinum surface, leading to the predominant formation of N_2 at low temperatures. At high temperatures, the amount of NO_{ad} grows [25c, 35] increasing the N_2O yield (Fig. S2). Considering the reaction scheme described above, it might be concluded that the

low-temperature peaks in the N_2/N_2O concentration curves are associated with the desorption of N_{ad} and NO_{ad} intermediates in the form of products, while the second peak is due to the steady-state reaction taking place at higher temperature.

The effect of Pt crystallite size on N_2 selectivity in the NH_3 oxidation reaction is rather weak (Fig. 6). The difference in S_{N2} values in the range of ~275–400°C is 10% for Pt/Al_2O_3 catalysts with platinum particles of ~1, ~2.6, and ~8 nm. Larger Pt particles show higher N_2 selectivity due to a large number of terraces on the surface.[25c] Note that higher S_{N2} was found at T <200°C over smaller Pt crystallites.[8a] It was explained by a decreased concentration of active oxygen on the surface of small crystallites, leading to a decreased specific activity and an increased N_2 selectivity. However, at T>200°C, the dependence of N_2 selectivity on the particle size Pt revealed the opposite trend.

Implications for NH_3 oxidation catalyst development.

The obtained results suggest that in order to obtain active and stable ammonia slip catalysts metallic Pt nanoparticles larger than 1 nm (at the same time, not too large, ideally of approx. 3 nm to use Pt efficiently [11c]) must be prepared. Sintering and redispersion of Pt (which would result in oxidation of formed small Pt species making them inactive) should be prevented. Ways of achieving this are required to ensure stability of the catalysts. Also keeping metallic Pt surface free of potentially poisoning surface species is vital to achieve high activity at low temperatures. Both conditions can be fulfilled via encapsulating Pt NPs in inorganic oxide supports. One strategy to produce such catalysts involves direct NP synthesis and stabilization in the pores of hierarchical (micro-mesoporous) zeolites as demonstrated for CO oxidation Pt [37] and CH_4 oxidation Pd catalysts.[38] Another viable strategy involves synthesis of a protective zeolite shell on top of Pt nanoparticles rendering an active and stable core-shell catalyst.[39] In both cases the zeolite can be functionalized with transition metals active in NH_3-SCR and play a role of the SCR catalyst layer in close proximity to Pt sites reducing the complexity of the monolith washcoating procedure. Both strategies are proved to be working, however the catalyst synthesis procedure becomes more complex. Whether benefits of more stable catalysts and simpler washcoating actually outweigh the cost of the more complex catalyst synthesis depends on the exact application scenario.

Conclusions

A study of Pt/Al_2O_3 catalysts for NH_3 oxidation was performed using a combination of structural, spectral, and catalytic methods. Catalysts with varied Pt state (metallic or oxidized) and Pt dispersion (particle size from ~1 to ~23 nm) were prepared.

It has been shown that a prereduced catalyst containing metallic Pt particles has significantly higher activity in the ammonia oxidation than the preoxidized one with a similar dispersion of Pt. The difference in the T_{50} value for oxidized and metallic platinum particles was more than 50°C. It was established that N_2 selectivity (S_{N2}) at T>270°C (corresponding to 100% NH_3 conversion) weakly depended on the Pt state. Below 270°C, the preoxidized PtO_x/γ-Al_2O_3 catalyst showed higher S_{N2} value in the comparison with the prereduced Pt^0/γ-Al_2O_3. This difference in S_{N2} can be explained by the increased contribution of N_2O

formed during desorption of surface intermediates of oxidative ammonia dehydrogenation from the metallic surface. Such intermediates may inhibit adsorption of O_2, while their removal provides Pt surface sites available for the efficient NH_3 oxidation with the formation of N_2 and N_2O at relatively low temperatures.

It was shown that the most significant improvement in catalytic activity took place when the size of Pt metallic particles was increased from ~1 to ~8 nm. In this case, the T_{50} value decreased by 28°C, while the TOF value increased by 30 times. A further increase in the size of metallic Pt particles (up to ~23 nm) did not lead to additional activity improvement. It was found that the N_2 selectivity during NH_3 oxidation over Pt/Al_2O_3 catalysts was mainly determined by the reaction temperature. At temperatures above 225°C, large Pt^0 particles (8-23 nm) demonstrated 10% higher N_2 selectivity than ~1 nm particles. Below 225°C, a slight increase in S_{N2} along with the decreasing Pt crystallite size was observed.

The influence of the reaction mixture on the catalytic properties has been studied through repeated heating/cooling cycles. In the case of the preoxidized Pt/Al_2O_3 catalyst with highly dispersed Pt species, an increase in activity as a result of the exposure to the reaction mixture was revealed. It was associated with the presence of Pt^{4+}/Pt^{2+} species on the catalyst surface. In this case, the metallic Pt was not observed, and the average size of Pt particles was almost unchanged after tests. In the case of prereduced catalysts containing Pt^0 particles, deactivation was observed during catalytic measurements due to the increase of Pt dispersion and partial Pt oxidation. The redispersion of large metallic particles may occur due to formation of volatile PtO_2 species. PtO_2 species can result from oxidation of surface of metallic particles at elevated temperature and under high O_2 pressure. In this case the volatile PtO_2 species can be trapped by defect alumina surface leading to the appearance of additional highly dispersed species.

Additional measurements were carried out in a realistic reaction mixture containing H_2O and CO_2. The addition of H_2O and CO_2 was accompanied by a slight shift of the NH_3 conversion curves towards higher temperatures (ΔT_{50} <15°C), while the trends of the activity and selectivity of Pt/Al_2O_3 catalysts on the Pt dispersion and Pt state were completely preserved.

Experimental Section

Catalyst Preparation

2 wt.% Pt/γ-Al_2O_3 catalysts were prepared by incipient wetness impregnation using aqueous solutions of hexachloroplatinic acid or platinum nitrate. Alumina support was obtained by air-calcination of Pural SCF-55 aluminum hydroxide (Boehmite Al(OH)O, Sasol) at 750°C for 4 hours.

A solution of platinum nitrate was obtained by dissolving $H_2[Pt(OH)_6]$ in water at 50-80°C using nitrogen dioxide.[40] A weak stream of NO_2 was passed through a pale yellow suspension of $H_2[Pt(OH)_6]$ in water at 50-70°C with constant stirring. The NO_2 flow was not stopped until the precipitate was completely dissolved and the color of the solution turned greenish. After 24 hours, the solution color changed to yellow-orange due to the oxidation of nitrosyl ligands in the platinum complex. No further changes to the solution occurred. The impregnation was carried out at room temperature (RT) with subsequent drying at RT (for 16 h), 60°C (for 1 h) and 120°C (for 2 h). Then, the obtained powder was air-calcined at 400°C (for 4 h). Part of the catalyst was additionally calcined in air at 600°C (for 4 h).

Similarly, catalysts were prepared using H_2PtCl_6 as a precursor (followed by calcination in air at 400°C). The air-calcined samples were prereduced

in H_2 at 350°C (for 2 h) and calcined at 400, 550, or 600°C in Ar (for 6 h). Then, the catalysts were washed from chlorine ions with aqueous ammonia and distilled water. The washed catalysts were sequentially dried in air at RT (for 16 h), 60°C (for 1 h) and 120°C (for 2 h) and, finally, calcined in argon at 400°C (for 2 h).

The final catalysts are denoted as N/Cl-Ox/Red-T, where N/Cl is $Pt(NO_3)_x$ or H_2PtCl_6, Ox/Red is the oxidative or reductive pretreatment, and T is the temperature of the final pretreatment.

X-ray diffraction (XRD)

X-ray diffraction patterns were obtained on a Bruker D8 diffractometer (Germany) using CuK_α radiation. To record the signal, a one-dimensional LynxEye detector was used. The measurement was carried out in the range of angles 2θ = 15-90° with a step of 0.05° and acquisition time per point of 5 s. For phase analysis, the ICDD PDF-2 database was used. The refinement of the structure and profile analysis were performed in the TOPAS software package.[41] The γ-Al_2O_3 phase was described by a set of corresponding reflections; the phase of metallic Pt was described by the Rietveld method. The crystallite size (D) was calculated using LVol-IB values (i.e., volume-weighted mean column lengths based on integral breadth).

Transmission Electron microscopy (TEM)

TEM investigation was performed using a Cs-corrected JEOL JEM-2200FS electron microscope installed at the "VTAN" resource center of Novosibirsk State University, Russia; and a Thermo Fisher Scientific Themis Z double Cs-corrected electron microscope installed at the Boreskov Institute of Catalysis, Russia. Both microscopes operated at an accelerating voltage of 200 kV, the spatial lattice resolution was 1.0 Å and 0.7 Å, correspondingly. Bright field images (BF-TEM) were acquired in traditional transmission mode. Dark field images were acquired in Scanning mode (STEM) using High-Angle Annular Dark-Field detectors (HAADF). Particle size distribution diagrams were obtained using "ImageJ" software.[42] To determine the size of the irregularly shaped particles, the diameter of a circle having the same projected area as the particle was determined. The samples for the TEM study were dispersed in ethanol in an ultrasonic bath and supported on a holey carbon film mounted on a copper grid. The average Pt particle size was obtained using OriginPro8 software. This analysis provides descriptive statistics about the data such as mean, standard deviation, minimum, maximum, and more.

X-ray photoelectron spectroscopy (XPS)

The X-ray photoelectron spectroscopy (XPS) was applied using an ES-300 (KRATOS Analytical, UK) spectrometer. A non-monochromatic MgKα source (hv=1253.6 eV) was used for electron emission. The core-level spectra of bulk metallic gold and copper with reference values $E_b(Au4f_{7/2})$ = 84.0 eV and $E_b(Cu2p_{3/2})$ = 932.7 eV were used for the spectrometer calibration [43]. In accordance with literature data for γ-Al_2O_3, the Al2p line with a binding energy E_b=74.5 eV was used as an internal standard for calibration of the spectra [43].

The ratio of aluminum and platinum atomic concentrations on the surface (Pt_{at}/Al_{at}) was estimated from the areas of the corresponding core-level spectra taking into account the atomic sensitivity factors [44]. Cl2p spectra were acquired to check for the residual chlorine in the catalysts prepared using H_2PtCl_6. For all samples surface Cl content was negligible. Pt4f spectra were used to analyze the charge state of platinum after the subtraction of the Al2p signal. The detailed description of the extraction of Pt4f signal from overlapping Pt4f+Al2p spectral lines can be found elsewhere [24]. Spectral processing was performed using XPS-Calc program, developed at the Boreskov Institute of Catalysis, and tested previously on a number of the metal-oxide catalytic systems [16, 45].

Measurement of catalytic activity in a model reaction mixture, TPD-NH₃

The measurements were carried out in an automated setup (setup #1) with a plug flow quartz reactor using a temperature-programmed reaction

of NH₃ oxidation (TPR-NH₃+O₂) and temperature-programmed desorption of NH₃ (TPD-NH₃). The catalyst grain size was 0.14-0.25 mm. Concentrations of NH₃, N₂O, NO, NO₂ were determined using an I1801 FTIR spectrometer (MIDAC corp., USA). Concentrations of O_2 and N_2 were determined using gas chromatography (Crystal-2000M, CHROMATEC, Russia). Before measurements, the catalysts were pretreated in a mixture of 20%O₂/He or in pure He at 400°C for 2 h. The pretreatment reaction medium was 20%O₂/He for air-calcined samples and helium for Ar-calcined samples.

The catalyst weight was 0.145 g for catalytic activity study. The initial reaction mixture containing 0.1 vol. % NH₃ and 4 vol. % O_2 (He balance) was supplied at a flow rate of 500 cm^3/min at room temperature. The space velocity was 120,000 h^{-1}. The sample was heated twice in the reaction mixture to 400°C at a rate of 10°C/min with intermediate cooling to room temperature.

The catalyst weight used for TPD-NH₃ study was 0.2 g. The initial reaction mixture containing 0.1 vol. % NH₃ (He balance) was supplied at a flow rate of 500 cm^3/min at room temperature. After NH₃ concentration reached the initial value, the sample was purged with helium (500 cm^3/min) to a residual NH₃ concentration below 5 ppm. The sample was heated in He to 400°C at a rate of 10°C/min.

Catalytic measurements in a realistic reaction mixture

Tests were also carried out in a plug flow quartz reactor in setup #2. The initial reaction mixture contained 500 ppm NH₃ and 13%O₂ (balanced by N₂). Additionally, tests were carried out in a mixture containing 500 ppm NH₃, 13%O₂, 5%H₂O, and 10%CO₂ (balanced by N₂). The feed rate of the reaction mixture of 1050 cm^3/min corresponded to a space velocity of 600,000 h^{-1}. 25.2 mg of catalyst were diluted with SiC. The samples were heated twice in the reaction mixture of NH₃ + O_2 from room temperature to 400°C at a rate of 3°C/min with intermediate cooling to 50°C. In the third heating-cooling cycle, H₂O and CO₂ were added to the initial mixture. The analysis of the reaction composition at the outlet of the reactor was carried out using Multigas 2030 FTIR (MKS Instruments, USA). N₂ concentration was calculated taking into account the total N balance for all reaction products.

The calculation of NH₃ conversion, product selectivity (for N₂O, N₂, NO, and NO₂) was carried out according to the following expressions:

$$X_{NH_3} = \frac{C_{NH_3}^{inlet} - C_{NH_3}^{outlet}}{C_{NH_3}^{inlet}},$$

$$S_{N_2O} = \frac{2 \times C_{N_2O}}{2 \times C_{N_2O} + 2 \times C_{N_2} + C_{NO} + C_{NO_2}} \times 100\%,$$

$$S_{N_2} = \frac{2 \times C_{N_2}}{2 \times C_{N_2O} + 2 \times C_{N_2} + C_{NO} + C_{NO_2}} \times 100\%,$$

$$S_{NO} = \frac{C_{NO}}{2 \times C_{N_2O} + 2 \times C_{N_2} + C_{NO} + C_{NO_2}} \times 100\%,$$

$$S_{NO_2} = \frac{C_{NO_2}}{2 \times C_{N_2O} + 2 \times C_{N_2} + C_{NO} + C_{NO_2}} \times 100\%,$$

where X_{NH_3} – NH₃ conversion, $C_{NH_3}^{inlet}$ – inlet NH₃ concentration, $C_{NH_3}^{outlet}$ – outlet NH₃ concentration, C_{N_2O} – N₂O concentration, C_{N_2} - N₂ concentration, C_{NO} – NO concentration, C_{NO_2} – NO₂ concentration.

Rate of the catalytic reaction was calculated from the catalytic data obtained at low NH₃ conversions (from 0 to 20%) using the following expression:

$$W\left(\frac{mol}{mol \times s}\right) = \frac{C_{NH_3}^{inlet} \times X \times V_{RM}}{Pt(mol)},$$

where $C_{NH_3}^{inlet}$ is the initial concentration of NH₃ (vol.% divided by 100), X is the NH₃ conversion, V_{RM} is the reaction mixture rate (in mol/s), and Pt(mol) – Pt content (in moles).

Estimation of catalytic activity taking into an account Pt dispersion (turnover frequency - TOF) was calculated using the next expression:

$$TOF(s^{-1}) = \frac{W}{D_{TEM}}.$$

TEM-derived dispersion (D_{TEM}) were obtained using the equation:[46]

$$D_{TEM} = \left(1.483 \times \frac{\langle d^2 \rangle}{\langle d^3 \rangle} - 0.733 \times \frac{\langle d \rangle}{\langle d^3 \rangle} + \frac{0.121}{\langle d^3 \rangle}\right) * 100$$

Acknowledgements

[1]   P. Tennison, C. Lambert, M. Levin, SAE International 2004-01-2091, 2004.

[2]   R. M. Heck, R. J. Farrauto, Catalytic Air Pollution Control: Commercial Technology, 2nd Edition, New York: John Wiley & Sons, Inc, 2002.

[3]   M. Jabłońska, R. Palkovits, Appl. Catal. B: Environ. 2016, 181, 332-351.

[4]   A. Walker, Top. Catal. 2016, 59, 695-707.

[5]   L. Chmielarz, M. Jabłońska, RSC Adv. 2015, 5, 43408-43431.

[6]   (a) M. Colombo, I. Nova, E. Tronconi, G. Koltsakis, Top. Catal. 2013, 56, 177-181; (b) S. Shrestha, M. P. Harold, K. Kamasamudram, A. Yezerets, Catal. Today 2014, 231, 105-115.

[7]   (a) A. Scheuer, W. Hauptmann, A. Drochner, J. Gieshoff, H. Vogel, M. Votsmeier, Appl. Catal. B: Environ. 2012, 111-112, 445-455; (b) A. Scheuer, M. Votsmeier, A. Schuler, J. Gieshoff, A. Drochner, H. Vogel, Top. Catal. 2009, 52, 1847; (c) S. Shrestha, M. P. Harold, K. Kamasamudram, A. Yezerets, Top. Catal. 2013, 56, 182-186; (d) Y. Li, J. N. Armor, Appl. Catal. B: Environ. 1997, 13, 131-139; (e) N. I. Il'chenko, Russ. Chem. Rev. 1976, 45, 1119-1134.

[8]   (a) J. J. Ostermaier, J. R. Katzer, W. H. Manogue, J. Catal. 1974, 33, 457-473; (b) J. J. Ostermaier, J. R. Katzer, W. H. Manogue, J. Catal. 1976, 41, 277-292.

[9]   M. Machida, Y. Tokudome, A. Maeda, Y. Kuzuhara, T. Hirakawa, T. Sato, H. Yoshida, J. Ohyama, K. Fujii, N. Ishikawa, ACS Catal. 2020, 10, 4677-4685.

[10] (a) S. Gan, Y. Liang, D. R. Baer, M. R. Sievers, G. S. Herman, C. H. F. Peden, J. Phys. Chem. B 2001, 105, 2412-2416; (b) D. Srinivas, P. Ratnasamy, in Nanotechnology in Catalysis. Nanostructure Science and Technology. (Eds.: B. Zhou, S. Han, R. Raja, G. A. Somorjai), Springer, New York, 2007, pp. 183-220.

[11] (a) A. C. M. van den Broek, Technische Universiteit Eindhoven (Eindhoven), 1998; (b) D. P. Sobczyk, E. J. M. Hensen, A. M. de Jong, R. A. van Santen, Top. Catal. 2003, 23, 109-117; (c) A. Boubnov, S. Dahl, E. Johnson, A. P. Molina, S. B. Simonsen, F. M. Cano, S. Helveg, L. J. Lemus-Yegres, J.-D. Grunwaldt, Appl. Catal. B: Environ. 2012, 126, 315-325.

[12] T. K. Hansen, Ph.D. Thesis thesis, Technical University of Denmark (DTU) 2017.

[13] (a) M. Peuckert, H. P. Bonzel, Surf. Sci. 1984, 145, 239-259; (b) Z. R. Ismagilov, S. A. Yashnik, A. N. Startsev, A. I. Boronin, A. I. Stadnichenko, V. V. Kriventsov, S. Kasztelan, D. Guillaume, M. Makkee, J. A. Moulijn, Catal. Today 2009, 144, 235-250; (c) D. A. Svintsitskiy, L. S. Kibis, A. I. Stadnichenko, S. V. Koscheev, V. I. Zaikovskii, A. I. Boronin, ChemPhysChem 2015, 16, 3318-3324.

[14] A. V. Kalinkin, M. Y. Smirnov, A. I. Nizovskii, V. I. Bukhtiyarov, J. Electron Spectrosc. Relat. Phenom. 2010, 177, 15-18.

[15] (a) G. K. Wertheim, S. B. DiCenzo, Phys. Rev. B 1988, 37, 844-847; (b) F. Parmigiani, E. Kay, P. S. Bagus, C. J. Nelin, J. Electron Spectrosc. Relat. Phenom. 1985, 36, 257-267.

[16] D. A. Svintsitskiy, L. S. Kibis, A. I. Stadnichenko, E. M. Slavinskaya, A. V. Romanenko, E. A. Fedorova, O. A. Stonkus, D. E. Doronkin, V. Marchuk, A. Zimina, M. Casapu, J.-D. Grunwaldt, A. I. Boronin, ChemCatChem 2020, 12, 867-880.

[17] (a) C. B. Alcock, G. W. Hooper, Proceedings of the Royal Society of London. Series A, Mathematical and Physical Sciences 1960, 254, 551-561; (b) T. W. Hansen, A. T. DeLaRiva, S. R. Challa, A. K. Datye, Acc. Chem. Res. 2013, 46, 1720-1730; (c) T. R. Johns, R. S. Goeke, V. Ashbacher, P. C. Thüne, J. W. Niemantsverdriet, B. Kiefer, C. H. Kim, M. P. Balogh, A. K. Datye, J. Catal. 2015, 328, 151-164; (d) C.-B. Wang, C.-T. Yeh, J. Catal. 1998, 178, 450-456.

[18] S. Shrestha, M. P. Harold, K. Kamasamudram, Chem. Eng. J. 2015, 278, 24-35.

[19] (a) G. Bagnasco, J. Catal. 1996, 159, 249-252; (b) H. Sjövall, R. J. Blint, L. Olsson, J. Phys. Chem. C 2009, 113, 1393-1405.

[20] T. Shimizu, M. Hasegawa, M. Inagaki, Energy & Fuels 2000, 14, 104-111.

[21] M. J. Ungerer, D. Santos-Carballal, A. Cadi-Essadek, C. G. C. E. van Sittert, N. H. de Leeuw, J. Phys. Chem. C 2019, 123, 27465-27476.

[22] D. A. Svintsitskiy, L. S. Kibis, A. I. Stadnichenko, E. M. Slavinskaya, A. S. Zaguzin, A. V. Romanenko, E. A. Derevyannikova, O. A. Stonkus, A. I. Boronin, AIP Conference Proceedings 2019, 2143, 020028.

[23] E. Ogel, M. Casapu, D. E. Doronkin, R. Popescu, H. Störmer, C. Mechler, G. Marzun, S. Barcikowski, M. Türk, J. D. Grunwaldt, J. Phys. Chem. C 2019, 123, 5433-5446.

[24] D. A. Svintsitskiy, E. M. Slavinskaya, O. A. Stonkus, A. V. Romanenko, A. I. Stadnichenko, L. S. Kibis, E. A. Derevyannikova, A. A. Evtushkova, A. I. Boronin, J. Struct. Chem. 2019, 60, 919-931.

[25] (a) W. D. Mieher, W. Ho, Surf. Sci. 1995, 322, 151-167; (b) J. Pérez-Ramírez, E. V. Kondratenko, V. A. Kondratenko, M. Baerns, J. Catal. 2004, 227, 90-100; (c) H. Ma, W. F. Schneider, ACS Catal. 2019, 9, 2407-2414.

[26] M. Sun, J. Liu, C. Song, Y. Ogata, H. Rao, X. Zhao, H. Xu, Y. Chen, ACS Appl. Mater. Interfaces 2019, 11, 23102-23111.

[27] R. F. Hicks, H. Qi, M. L. Young, R. G. Lee, J. Catal. 1990, 122, 280-294.

[28] V. A. Drozdov, P. G. Tsyrulnikov, V. V. Popovskii, N. N. Bulgakov, E. M. Moroz, T. G. Galeev, React. Kinet. Catal. Lett. 1985, 27, 425-427.

[29] M. J. Lundwall, S. M. McClure, D. W. Goodman, J. Phys. Chem. C 2010, 114, 7904-7912.

[30] A. Y. Stakheev, D. A. Bokarev, I. P. Prosvirin, V. I. Bukhtiyarov, in Advanced Nanomaterials for Catalysis and Energy (Ed.: V. A. Sadykov), Elsevier, 2019, pp. 295-320.

[31] A. Boubnov, A. Gänzler, S. Conrad, M. Casapu, J.-D. Grunwaldt, Top. Catal. 2013, 56, 333-338.

[32] M. Niwa, K. Awano, Y. Murakami, Appl. Catal. 1983, 7, 317-325.

[33] P. Briot, A. Auroux, D. Jones, M. Primet, Appl. Catal. 1990, 59, 141-152.

[34] T. F. Garetto, C. R. Apesteguía, Appl. Catal. B: Environ. 2001, 32, 83-94.

[35] D. P. Sobczyk, J. van Grondelle, P. C. Thüne, I. E. Kieft, A. M. de Jong, R. A. van Santen, J. Catal. 2004, 225, 466-478.

[36] J. Liu, Q. Lin, S. Liu, S. Xu, H. Xu, Y. Chen, New J. Chem. 2020, 44, 4108-4113.

[37] J. Gu, Z. Zhang, P. Hu, L. Ding, N. Xue, L. Peng, X. Guo, M. Lin, W. Ding, ACS Catal. 2015, 5, 6893-6901.

[38] A. W. Petrov, D. Ferri, F. Krumeich, M. Nachtegaal, J. A. van Bokhoven, O. Kröcher, Nat. Commun. 2018, 9, 2545.

[39] R. S. Ghosh, T. T. Le, T. Terlier, J. D. Rimer, M. P. Harold, D. Wang, ACS Catal. 2020, 10, 3604-3617.

[40] I. E. Bekk, D. A. Konevets, V. I. Zajkovskij, F. V. Tuzikov, V. I. Bukhtijarov, №2352391, 2009.

[41] TOPAS, version 4.2., Bruker AXS Inc., 2009, Madison, Wisconsin, USA.

[42] C. A. Schneider, W. S. Rasband, K. W. Eliceiri, Nature Methods 2012, 9, 671.

[43] D. Briggs, Handbook of X-ray Photoelectron Spectroscopy C. D. Wanger, W. M. Riggs, L. E. Davis, J. F. Moulder and G. E. Muilenberg Perkin-Elmer Corp., Physical Electronics Division, Eden Prairie, Minnesota, USA, 1979. 190 pp.

[44] J. F. Moulder, W. F. Stickle, P. E. Sobol, K. D. Bomben, Handbook of X-ray photoelectron spectroscopy, Perkin-Elmer Corp, Eden Prairie, Minnesota, USA, 1992.

[45] (a) T. Y. Kardash, E. A. Derevyannikova, E. M. Slavinskaya, A. I. Stadnichenko, V. A. Maltsev, A. V. Zaikovskii, S. A. Novopashin, A. I. Boronin, K. M. Neyman, Frontiers in Chemistry 2019, 7, 114; (b) L. S. Kibis, D. A. Svintsitskiy, E. A. Derevyannikova, T. Y. Kardash, E. M. Slavinskaya, O. A. Stonkus, V. A. Svetlichnyi, A. I. Boronin, Appl. Surf. Sci. 2019, 493, 1055-1066.

[46] A. D. Allian, K. Takanabe, K. L. Fujdala, X. Hao, T. J. Truex, J. Cai, C. Buda, M. Neurock, E. Iglesia, J. Am. Chem. Soc. 2011, 133, 4498-4517.

Entry for the Table of Contents
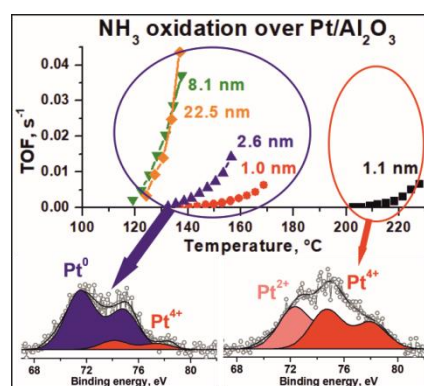
The fundamental for heterogeneous catalysis factors such as dispersion and metallic/oxidized states of platinum were investigated in the NH$_3$ oxidation over Pt/Al$_2$O$_3$ catalysts. For Pt^0, the catalytic activity can be improved by the increase of average particle size from ~1 to ~8 nm. PtO$_x$ species demonstrating significantly lower activity in the comparison with metallic Pt can be partially activated through the growth of Pt^{4+}/Pt^{2+} surface ratio.